Dual-energy Spectral CT Quantitative Parameters for the Differentiation of Glioma Recurrence from Treatment-Related Changes: A Preliminary Study

Yanchun Lv
Sun Yat-sen University Cancer Center
Jian Zhou
Sun Yat-sen University Cancer Center
Xiaofei Lv
Sun Yat-sen University Cancer Center
Li Tian
Sun Yat-sen University Cancer Center
Haoqiang He
Sun Yat-sen University Cancer Center
Zhigang Liu
Fifth Affiliated Hospital of Sun Yat-sen University
Yi Wu
Shantou Central Hospital
Lujun Han
Sun Yat-sen University Cancer Center
Meili Sun
Sun Yat-sen University Cancer Center
Yadi Yang
Sun Yat-sen University Cancer Center
Chengcheng Guo
Sun Yat-sen University Cancer Center
Cong Li
Sun Yat-sen University Cancer Center
Rong Zhang
Sun Yat-sen University Cancer Center
Chuanmiao Xie
Sun Yat-sen University Cancer Center
Yinsheng Chen
Sun Yat-sen University Cancer Center
Zhong-ping Chen (chenzhp@sysucc.org.cn)
https://orcid.org/0000-0002-6868-9866

Research article

Keywords: glioma, dual energy spectral CT, recurrence

Posted Date: October 14th, 2019

DOI: https://doi.org/10.21203/rs.2.15990/v1

Version of Record: A version of this preprint was published on January 16th, 2020. See the published version at https://doi.org/10.1186/s12880-019-0406-5.

Abstract

Background: Differentiating glioma recurrence from treatment-related changes can be challenging on conventional imaging. We evaluated the use of dual-energy spectral computed tomographic (CT) quantitative parameters for this differentiation.

Methods: Twenty-eight patients were examined by dual-energy spectral imaging CT. The slope of the spectral Hounsfield unit curve (λ HU), effective atomic number (Z eff), normalized effective atomic number (Z eff-N), iodine concentration (IC), and normalized iodine concentration (IC N) in the post-treatment enhanced areas were calculated. Pathological results or clinicoradiologic follow-up of ≥2 months were used for final diagnosis. Nonparametric and t -tests were used to compare quantitative parameters between glioma recurrence and treatment-related changes. Positive predictive value (PPV), negative predictive value (NPV), and accuracy were calculated; sensitivity and specificity were calculated using receiver operating characteristic (ROC) curves. ROC curves were generated using predictive probabilities to evaluate the diagnostic value.

Results: There were no significant differences in quantitative parameters based on examination of pre-contrast λ HU , Z eff , Z eff-N , IC, IC N and venous phase IC N (P >0.05). Venous phase λ HU , Z eff , Z eff-N , and IC in glioma recurrence were higher than in treatment-related changes (P <0.001). The optimal venous phase threshold was 1.03, 7.75, 1.04, and 2.85 mg/cm 3 , achieving 66.7%, 91.7%, 83.3%, and 91.7% sensitivity; 100.0%, 77.8%, 88.9%, and 77.8% specificity; 100.0%, 73.3%, 83.3%, and 73.3% PPV; 81.8%, 93.3%, 88.9%, and 93.3% NPV; and 86.7%, 83.3%, 86.7%, and 83.3% accuracy, respectively. The areas under the curve (AUC) were 0.912, 0.912, 0.931, and 0.910 in glioma recurrence and treatment-related changes, respectively.

Conclusions: Dual-energy spectral CT imaging may provide quantitative values to aid in differentiation of glioma recurrence from treatment-related changes.

Background

Differentiating glioma recurrence from treatment-related changes (necrosis after operation or radiation, pseudoprogression after chemotherapy) remains a significant challenge. Clinically, the two entities have totally different consequences; however, both often share the same symptoms and show very similar features in conventional magnetic resonance imaging (MRI) and computed tomography (CT) [1,2]. It is crucial for clinicians to be able to differentiate these disparate outcomes, because the management strategies for tumor recurrence and treatment-related changes are entirely different [3].

Many advanced imaging techniques have been used in an attempt to distinguish glioma recurrence from treatment-related changes, such as positron emission tomography (PET), functional magnetic resonance imaging (fMRI), and single photon emission CT (SPECT). These techniques, however, are imperfect, and accurate differentiation of treatment-related changes remains difficult [2–8]

Gemstone spectral imaging (GSI) CT scanning mode, which uses dual energy x-rays produced by the rapid switching of low (80 kVp) and high (140 kVp) tube voltages was introduced [9]. GSI quantitative parameters have been used in the diagnosis of several kinds of tumors [9–13].

The purpose of this study was to explore the use of dual-energy gemstone spectral computed tomographic (CT) quantitative parameters for the differentiation of glioma recurrence from treatment-related changes.

Methods

Patients

This retrospective study was approved by the ethics committee at Sun Yat-sen University Cancer Center, and all included patients provided informed consent. A total of 28 patients (13 men and 15 women; mean age: 39.3 ± 13.0 years) who underwent brain dual-energy gemstone spectral CT were enrolled. All patients had undergone tumor operation, and the inclusion criteria were: (1) histological confirmation of the brain tumor as a glioma; (2) the primary treatments were operation, chemotherapy (temozolomide) or radiation therapy (total dose received from 40 to 60 Gy); and (3) subsequently developed new contrast-enhanced lesions could be detected in the field of treatment. The exclusion criteria were definite contraindications for contrast-agent administration, cardiopathy, or pregnancy. A final diagnosis of all included patients was determined based on either a second operation or a follow-up examination. The follow-up was confirmed at intervals of ≥2 months. For follow-up diagnosis, treatment-related changes were confirmed when the enhancing lesion entirely disappeared, partially resolved, or kept stable on subsequent follow-up images over a minimal of 2 months; and if the patient was in a stable clinical state and showed no new neurologic symptoms. The glioma recurrence was based on the development of neurologic symptoms and a progressive increase in the size of the enhancing lesion or a new enhancing lesion on follow-up examination. Two radiologists (YL and JZ, with 20 and 8 years of experience in radiology, respectively) assessed the images in consensus.

Dual energy Gemstone Spectral CT Examination

Images were obtained by the Discovery CT750HD scanner (GE Healthcare, Waukesha, Wis). All patients were scanned using the following parameters in the GSI mode: tube voltage of 140 kV and 80 kV, 0.5 ms instantaneous switch; tube current, 0–600 mA automatic modulation; the collimation thickness was 0.625 mm; the rotation speed was 0.8 s; and the helical pitch was 1.375. A total CT dose index volume was 18.28 mGy, which was 69.5% lower than the CT dose index volume of 59.89 mGy for average conventional head scanning at our institution. An iodinated nonionic contrast agent (iopamidol 300; Bracco, Milan, Italy) was injected at 2.8 mL/s and 1.5 ml/kg through the right ulnar vein by an automated injector. The venous phase delay times for the scan were 50 s.

GSI Quantitative Parameters Acquisition

The images of GSI data were managed by software (GSI viewer 4.5, GE Healthcare). The region of interest (ROI) was drawn on the pre-contrast scan and the reconstructed monochromatic venous phase data images on 70-keV. The ROI was targeted for most suspicious areas of tumor recurrence with nodular enhancement, with care to exclude calcification and minute vessel. The same ROI was copied on the other common brain parenchyma as a contrast. The effective atomic number (Z_{eff}) and the iodine concentration (IC) CT values in monochromatic images and iodine-based material-decomposition images for each ROI were automatically calculated (Figures

1a, 1b). All of the ROIs were automatically copied on all monochromatic images and iodine-based material-decomposition images. Two radiologists independently performed the measurements.

Data Processing and Statistical Analysis

Z_{eff}, IC (in milligrams per milliliter), and CT values on 40–140-keV monochromatic images were calculated and exported by the average values of two radiologists. The Z_{eff} of the glioma ($Z_{eff\text{-}gli}$) and IC of the glioma (IC_{gli}) were normalized to values in the normal reference brain parenchyma ($Z_{eff\text{-}BP}$ and IC_{BP}) to derive a normalized Z_{eff} ($Z_{eff\text{-}N}$) and a normalized IC (IC_N): $Z_{eff\text{-}N} = Z_{eff\text{-}gli}/Z_{eff\text{-}BP}$ and $IC_N = IC_{gli}/IC_{BP}$, where BP is the normal reference brain parenchyma. The slope of the Hounsfield unit curve (λ_{HU}) was presented by the differences between the CT value on 40 keV and that on 70 keV divided by the energy difference (30 keV): $\lambda_{HU} = (40\ keV_{HU} - 70\ keV_{HU})/30$ keV (Figure 1c).

Quantitative data were saved as means and standard deviation (*x s)* or medians with interquartile range. All the GSI quantitative parameters were compared by two independent samples *t* test and nonparametric test. ROC curves were then generated by using predictive probabilities to evaluate the diagnostic value. Negative predictive value (NPV), positive predictive value (PPV), and accuracy were also calculated. The maximum Youden's index was chosen as the best threshold. Data were analyzed using statistical software package (SPSS version 21.0; SPSS Inc., Chicago, IL), and a *P* value of <0.05 was considered to indicate statistical significance.

Results

Clinical and pathological results

A total of 28 patients were examined with dual energy gemstone spectral CT. Fifteen women [mean age, 36.9 ± 10.6 years] and 13 men [mean age, 42.2 ± 15.3 years] were included in the final analysis. A total of 30 lesions (12 glioma recurrence lesions, 18 treatment-related change lesions) were enrolled for evaluation.

The primary histopathology as per WHO 2007 classification was 15 Grade II (53.6%), 7 Grade III (25%), 6 Grade IV (21.4%). The primary histopathology was 6 glioblastomas (21.4%), 8 astrocytomas (28.6%), 3 anaplastic astrocytomas (10.7%), 2 oligodendrogliomas (7.1%), 3 anaplastic oligodendrogliomas (10.7%), 3 oligoastrocytomas (10.7%), 2 anaplastic oligoastrocytomas (7.1%), 1 ganglioglioma (3.6%). The primary treatments were 3 operation only (10.7%); 5 operation and radiation therapy (17.9%); 20 operation, radiation therapy, and chemotherapy (71.4%).

Pathology after operation showed glioma recurrence in 5 patients (5 lesions) and treatment-related changes in 2 patients (2 lesions). The recurrence group of second histopathology showed 2 glioblastomas (Grade IV), 1 astrocytoma (Grade II), 1 anaplastic oligodendroglioma (Grade III), 1 and anaplastic oligoastrocytoma (Grade III).

Six patients (7 lesions) without pathologic evaluation were finally classified into the glioma recurrence group up to a median period of 5 months (range, 2–24 months). Fifteen patients (16 lesions) without pathologic

evaluation were finally classified into the treatment-related changes group up to a median period of 7.5 months (range, 2–46 months). Patient characteristics are listed in Table 1.

GSI Quantitative Parameters for Differentiating glioma recurrence from treatment-related changes

The differences in the dual-energy spectral CT imaging quantitative parameters between glioma recurrence and treatment-related changes are listed in Table 2. There were no significant differences in quantitative parameters based on examination of pre-contrast λ_{HU}, Z_{eff}, $Z_{eff\text{-}N}$, IC, IC_N and venous phase IC_N ($P > 0.05$) on dual-energy spectral CT images. The mean λ_{HU} ($P < 0.001$) for glioma recurrence was 1.426 ± 0.762 vs. 0.314 ± 0.373 for treatment-related changes in the venous phase. In addition, the Z_{eff} ($P < 0.001$) for glioma recurrence was 8.034 ± 0.238 vs. 7.671 ± 0.151 for treatment-related changes in the venous phase. Similarly, the $Z_{eff\text{-}N}$ ($P < 0.001$) for glioma recurrence was 1.058 ± 0.020 vs. 1.013 ± 0.024 for treatment-related changes. The IC ($P < 0.001$) for glioma recurrence was 7.319 ± 3.967 vs. 1.703 ± 2.049 for treatment-related changes in the venous phase (Figure 2). The optimal venous phase λ_{HU}, Z_{eff}, $Z_{eff\text{-}N}$, and IC threshold was 1.03, 7.75, 1.04, and 2.85 mg/cm^3, achieving a sensitivity of 66.7%, 91.7%, 83.3%, and 91.7%; specificity of 100.0%, 77.8%, 88.9%, and 77.8%; PPV of 100.0%, 73.3%, 83.3%, and 73.3%; NPV of 81.8%, 93.3%, 88.9%, and 93.3%; and accuracy of 86.7%, 83.3%, 86.7%, and 83.3%, respectively (Table 3). The areas under the curve (AUC) were 0.912, 0.912, 0.931, and 0.910 in glioma recurrence and treatment-related changes, respectively (Figure 3).

Discussion

A high incidence of treatment-related changes has been noted in patients who undergo post-operative radiotherapy or combined chemoradiotherapy with temozolomide. Moreover, routinely available CT and MRI techniques do not allow a reliable distinction between glioma recurrence and treatment-related changes [1, 14]. Further, a new contrast-enhancing lesion observed on follow up imaging is often a mixture of necrotic tissue and growing tumor, which this adds to the complexity of lesion characterization [3].

In this study, we used dual-energy spectral CT quantitative parameters to differentiate glioma recurrence from treatment-related changes. In addition, we found the slope of λ_{HU}, Z_{eff}, $Z_{eff\text{-}N}$, and IC in the venous phase to be higher in patients with glioma recurrence than in those with treatment-related changes.

The λ_{HU} value could be automatically generated for given ROIs, describing the dynamic changes of measured CT Hounsfield units of ROIs against increasing keV values within the range of 40 to 140 keV [10]. In our study, we calculated λ_{HU} as the differences between the CT value on 40 keV and that on 70 keV divided by the energy difference (30 keV). Our results showed that the venous phase λ_{HU} in glioma recurrence was higher than in treatment-related changes, indicative of feasibility of enhancing venous phase λ_{HU} as a differentiating factor. Receiver operating characteristic analysis in our study revealed that the venous phase λ_{HU} was highly specific (100%) for differentiating glioma recurrence from treatment-related changes. These findings were similar to the findings in previous reports [10, 13]. Srinivasan et al. also reported that the spectral HU curve is a promising parameter for differentiating benign and malignant neck pathologic findings [15].

Z_{eff} is another quantitative index to characterize nodule composition. Z_{eff} represents the composite atom for a compound or mixture of various materials and is important to predict how x-rays interact with a substance [10]. According to our study results, venous phase Z_{eff} and $Z_{eff\text{-}N}$ were higher in glioma recurrence than in treatment-related changes, which was indicative of the feasibility of venous phase Z_{eff} and $Z_{eff\text{-}N}$ as a differentiating factor; these results are consistent with the findings in previous reports [10, 13]. The ROC analysis in our study revealed that the venous phase Z_{eff} was highly sensitive in differentiating glioma recurrence from treatment-related changes.

Lv et al. tested tubes filled with known iodine concentrations and iodine concentrations measured from the iodine-based material-decomposition images, reported a linear relationship between the measured and actual concentrations [9]. According to our study results, venous phase IC was higher in glioma recurrence than in treatment-related changes, indicative of feasibility of venous phase IC as a differentiating factor. The ROC analysis in our study revealed that the venous phase IC was highly sensitive for differentiating glioma recurrence from treatment-related changes. A previous report also suggested that IC in thyroid nodules can be used as a quantitative parameter to distinguish malignant from benign nodules [10]. Furthermore, the measured IC in lesions might be a useful quantitative parameter that reflects the blood supply to lesions [11, 12]. Moding et al. showed that dual energy CT is a powerful tool for monitoring vascular changes after radiation therapy [16]. Changes in tumor-associated vascular patterns and increase in the number of blood vessels may contribute to increases in IC [17].

In our study, there were no significant differences in the quantitative parameters of venous phase IC_N, contradicted with venous phase IC. This may be because of the following reasons. First, the sample size was relatively small. Second, gliomas are a heterogeneous group of tumors, which sometimes showed up as poor soft tissue contrast on dual-energy spectral CT, leading to potential selection bias.

There are a few other limitations to this study. In our experience, the differential diagnosis for lesions near the skull base was relatively challenging owing to many small blood vessels on the cerebral cortex; this might have led to inaccuracies in differential diagnosis. Second, it is important to note that not all glioma recurrence lesions in the present series were analyzed at biopsy; some cases were confirmed by follow-up. This may have influenced the study results. Third, we do not have data on inter observer reliability, because the readers assessed the images in consensus. Finally, we did not consider tumor heterogeneity and spatial heterogeneity. Hence, further large-scale prospective trials, with glioma classification and tumor heterogeneity are required to validate our results by dual-energy spectral imaging.

Conclusion

In conclusion, dual energy spectral CT imaging may potentially provide quantitative values to aid the differentiation of glioma recurrence from treatment-related changes. Thus, a dual-energy spectral CT would mean a second examination in addition to the routine MRI in clinical practice.

Abbreviations

GSI = gemstone spectral imaging; λ_{HU} = the slope of the spectral Hounsfield unit curve; Z_{eff} = effective atomic number; $Z_{eff\text{-}N}$ = normalized effective atomic number; IC = iodine concentration; IC_N = normalized iodine concentration

Declarations

Acknowledgements

Not applicable.

Authors' contributions

YL, JZ, YC and ZC conceived and designed research; XL, LT, HH, ZL, YW, LH, MS, and YY collected data and conducted research; CG, CL, RZ, and CX analyzed and interpreted data; JZ wrote the initial paper; ZC revised the paper; YL and ZC had primary responsibility for final content. All authors read and approved the final manuscript.

Funding

This study was funded by National Basic Research Program of China (973 Program, grant number 2015CB755500); Science and Technology Planning Project of Guangdong Province, China (grant number 2012B031800102, 2016A020213004); Guangzhou Science and Technology Program key projects (grant number 201803010056); National Natural Science Foundation of China (grant number 81572500); and Hunan Young Talents (grant number 2016RS3036). All of them play a role in the design of the study and collection, analysis, and interpretation of data and in writing the manuscript.

Availability of data and materials

The datasets generated and analyzed during the current study are available from the corresponding author on reasonable request.

Ethics approval and consent to participate

The written consents were obtained from the patients or the relatives of patients. The study was approved by the Ethics Committee of the Sun Yat-sen University Cancer Center.

Consent for publication

All data published here are under the consent for publication.

Competing interests

The authors declare that they have no competing interests.

Author details

[1]Department of Medical Imaging, Sun Yat-sen University Cancer Center, State Key Laboratory of Oncology in South China, Collaborative Innovation Center for Cancer Medicine, 651 Dongfeng Road East, Guangzhou 510060, China

[2]Department of head and neck oncology, Phase 1 clinical trial ward, The cancer center of the fifth affiliated hospital of Sun Yat-sen University, Zhuhai, 519001, China.

[3]Department of Radiology, Shantou Central Hospital, No.114 Waima Road, Shantou, 515041 Guangdong, China

[4]Department of Neurosurgery/Neuro-oncology, Sun Yat-sen University Cancer Center, State Key Laboratory of Oncology in South China, Collaborative Innovation Center for Cancer Medicine, 651 Dongfeng Road East, Guangzhou 510060, China

References

1. Brandsma D, Stalpers L, Taal W, Sminia P, van den Bent MJ. Clinical features, mechanisms, and management of pseudoprogression in malignant gliomas. The Lancet Oncology. 2008;9:453–61.
2. Zhang H, Ma L, Wang Q, Zheng X, Wu C, Xu B. Role of magnetic resonance spectroscopy for the differentiation of recurrent glioma from radiation necrosis: a systematic review and meta-analysis. Eur J Radiol. 2014;83:2181–9.
3. Verma N, Cowperthwaite MC, Burnett MG, Markey MK. Differentiating tumor recurrence from treatment necrosis: a review of neuro-oncologic imaging strategies. Neuro Oncol. 2013;15:515–34.
4. Chao ST, Ahluwalia MS, Barnett GH, Stevens GHJ, Murphy ES, Stockham AL, et al. Challenges with the diagnosis and treatment of cerebral radiation necrosis. Int J Radiat Oncol Biol Phys. 2013;87:449–57.
5. Enslow MS, Zollinger LV, Morton KA, Kadrmas DJ, Butterfield RI, Christian PE, et al. Comparison of 18F-fluorodeoxyglucose and 18F-fluorothymidine PET in differentiating radiation necrosis from recurrent glioma. Clin Nucl Med. 2012;37:854–61.
6. Pyka T, Gempt J, Ringel F, Hüttinger S, van Marwick S, Nekolla S, et al. Prediction of glioma recurrence using dynamic 18F-fluoroethyltyrosine PET. AJNR Am J Neuroradiol. 2014;35:1924–9.
7. Shah R, Vattoth S, Jacob R, Manzil FF, O'Malley JP, Borghei P, et al. Radiation necrosis in the brain imaging features and differentiation from tumor recurrence. Radiographics. 2012;32:1343–59.
8. Kim HS, Goh MJ, Kim N, Choi CG, Kim SJ, Kim JH. Which combination of MR imaging modalities is best for predicting recurrent glioblastoma? Study of diagnostic accuracy and reproducibility. Radiology. 2014;273:831–43.
9. Lv P, Lin XZ, Li J, Li W, Chen K. Differentiation of small hepatic hemangioma from small hepatocellular carcinoma: recently introduced spectral CT method. Radiology. 2011;259:720–29.

10. Li M, Zheng X, Li J, Yang Y, Lu C, Xu H, et al. Dual-energy computed tomography imaging of thyroid nodule specimens comparison with pathologic findings. Invest Radiol. 2012;47:58–64.
11. Zhang XF, Lu Q, Wu LM, Zou AH, Hua XL, Xu JR. Quantitative iodine-based material decomposition images with spectral CT imaging for differentiating prostatic carcinoma from benign prostatic hyperplasia. Acad Radiol. 2013;20:947–56.
12. Yu Y, Lin X, Chen K, Chai W, Hu S, Tang R, et al. Hepatocellular carcinoma and focal nodular hyperplasia of the liver: differentiation with CT spectral imaging. European Radiology. 2013;23:1660–8.
13. Liu X, Ouyang D, Li H, Zhang R, Lv Y, Yang A, ea al. Papillary thyroid cancer: dual-energy spectral CT quantitative parameters for preoperative diagnosis of metastasis to the cervical lymph nodes. Radiology. 2015;275:167–76.
14. Jena A, Taneja S, Jha A, Damesha NK, Negi P, Jadhav GK, et al. Multiparametric evaluation in differentiating glioma recurrence from treatment-induced necrosis using simultaneous 18F-FDG-PET/MRI: a single-institution retrospective study. AJNR Am J Neuroradiol. 2017;38:899–907.
15. Srinivasan A, Parker RA, Manjunathan A, Ibrahim M, Shah GV, Mukherji SK. Differentiation of benign and malignant neck pathologies preliminary experience using spectral computed tomography. J Comput Assist Tomogr. 2013;37:666–72.
16. Moding EJ, Clark DP, Qi Y, Li Y, Ma Y, Ghaghada K, et al. Dual-energy micro-computed tomography imaging of radiation-induced vascular changes in primary mouse sarcomas. Int J Radiat Oncol Biol Phys. 2013;85:1353–9.
17. Vogl TJ, Schulz B, Bauer RW, Stöver T, Sader R, Tawfik AM. (2012) Dual-energy CT applications in head and neck imaging. AJR Am J Roentgenol. 2012;199:S34–9.

Tables

Table 1: Patient characteristics

Characteristic	Value
Age (mean years)	39.3 ± 13.0
Sex (No. of patients) (%)	
Male	13 (46.4)
Female	15 (53.6)
WHO classification (No. of lesions) (%)	
Grade II	15 (53.6)
Grade III	7(25.0)
Grade IV	6 (21.4)
Primary treatment (No. of patients) (%)	
Operation	3(10.7)
Operation + radiation therapy	5 (17.9)
Operation + radiation therapy + chemotherapy	20 (71.4)
Final diagnosis (No. of lesions) (%)	
Recurrence	11 (39.3)
Pathologic	5 (17.9)
Clinicoradiologic follow up	6 (21.4)
Treatment related changes	17 (60.7)
Pathologic	2 (7.1)
Clinicoradiologic follow up	15 (53.6)

Table 2: Difference of GSI quantitative parameters between glioma recurrence and treatment-related changes

GSI quantitative parameters	glioma recurrence	treatment related changes	*P* Value
Precontrast λ_{HU}	-0.007(-0.477, 0.494)	-0.064(-0.619, 0.310)	0.859
Precontrast Z_{eff}	7.545(7.353, 7.745)	7.520(7.295, 7.653)	0.723
Precontrast Z_{eff-N}	1.007(0.996, 1.012)	1.005(0.997, 1.012)	0.965
Precontrast IC	-0.108(-2.598, 2.649)	-0.375(-3.33, 1.428)	0.790
Precontrast IC_N	0.733(0.509, 1.102)	0.969(0.504, 1.086)	0.723
Venous phase λ_{HU}	1.426 ± 0.762	0.314 ± 0.373	<0.001
Venous phase Z_{eff}	8.034 ± 0.238	7.671 ± 0.151	<0.001
Venous phase Z_{eff-N}	1.058 ± 0.020	1.013 ± 0.024	<0.001
Venous phase IC	7.319 ± 3.967	1.703 ± 2.049	<0.001
Venous phase IC_N	0.636(-2.140, 3.514)	0.827(-0634, 1.740)	0.832

Notes: All *P* values for group comparisons were obtained by *t* test.

* Data in parentheses are medians with interquartile range.

Table 3: GSI quantitative parameters for differential diagnosis of glioma recurrence and treatment-related changes

GSI Quantitative Parameters	AUC	Maximum Youden Index	Threshold of Parameters	Sensitivity (%)	Specificity (%)	PPV (%)	NPV (%)	Accuracy
Venous phase λ_{HU}	0.912(0.812,1.012)	0.667	1.03	66.7(56.7,76.7)	100.0(90.0,110.0)	100.0(90.0,110.0)	81.8(71.8.91.8)	86.7(76.7,96.7)
Venous phase Z_{eff}	0.912(0.810,1.014)	0.695	7.75	91.7(81.5,101.9)	77.8(67.6,88.0)	73.3(63.1,83.5)	93.3(83.1,103.5)	83.3(73.1,93.5)
Venous phase Z_{eff-N}	0.931(0.843,1.019)	0.722	1.04	83.3(74.5,92.1)	88.9(80.1,97.7)	83.3(74.5,92.1)	88.9(80.1,97.7)	86.7(77.9,95.5)
Venous phase IC	0.910(0.810, 1.010)	0.695	2.85	91.7(81.9,101.5)	77.8(68.0,87.6)	73.3(63.5,83.1)	93.3(83.5,103.1)	83.3(73.5,93.1)

Abbreviations: AUC = area under the receiver operating characteristic curve.

*Data in parentheses are 95% confidence intervals (CIs).

Figures

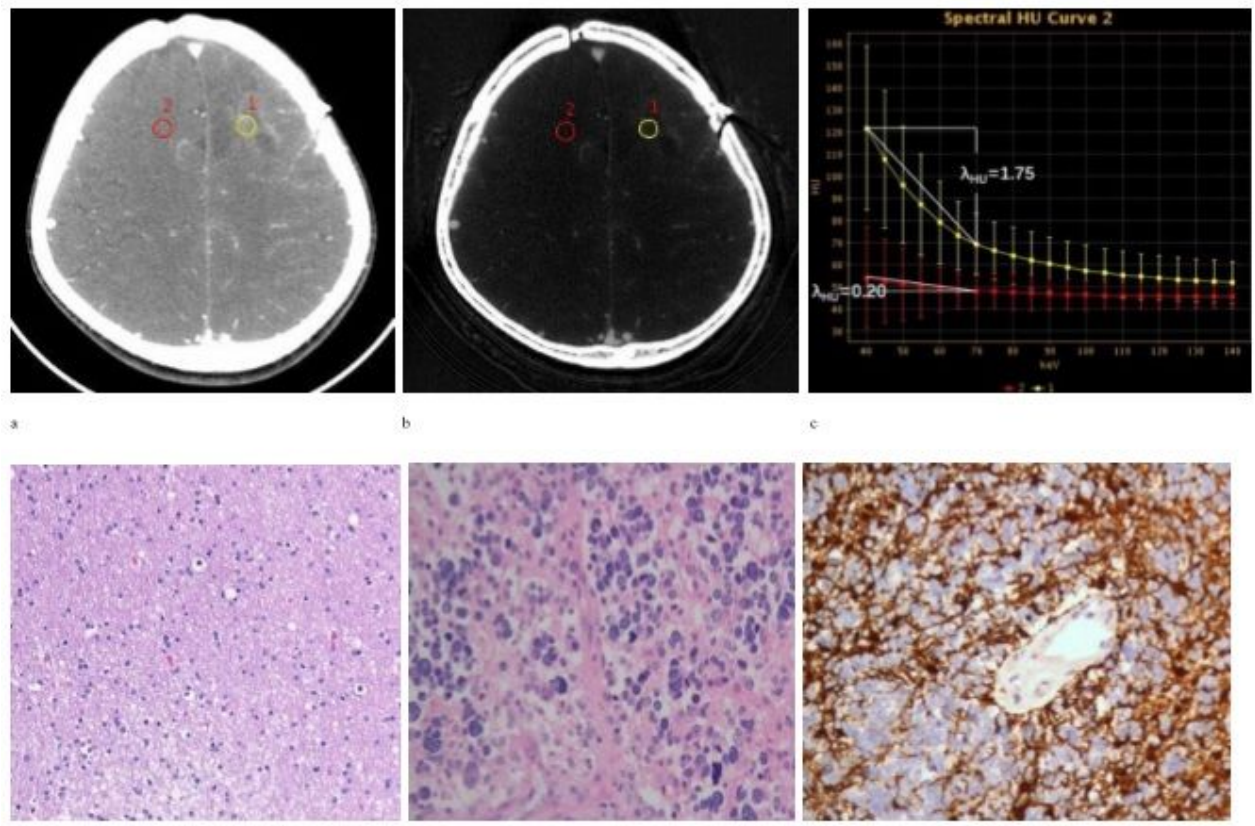

Figure 1

Contrast-enhanced venous phase GSI images show that IC and spectral curve were significantly different in glioma recurrence and the normal reference brain parenchyma. (a) Contrast-enhanced 70-keV monochromatic image (L1: area, 54.16 mm2; mean CT value, 69.33 HU; L2: 54.16 mm2; mean CT value, 48.06 HU). (b) Iodine-based materialdecomposition image shows that IC in glioma recurrence and the normal reference brain parenchyma were 0.915 mg/cm3 and 0.113 mg/cm3 (L1: area, 54.16 mm2; mean IC, 9.15 · 100 μg/cm3; L2: area, 54.16 mm2; mean IC, 1.13 · 100 μg/cm3). (c) Graph shows spectral HU curve of glioma recurrence (yellow) and the normal reference brain parenchyma (red), slope of the curve representing glioma recurrence is much higher than the normal reference brain parenchyma (1.75 vs. 0.20). (d) The pathology noted after the first operation indicated astrocytoma (Grade II). (e) A large of tumor cells showed diffused distribution in the smear; eosinophil, nuclear were marked atypia, and the pathologic diagnosis was glioblastoma (Grade IV). (f) The GFAP was positive.

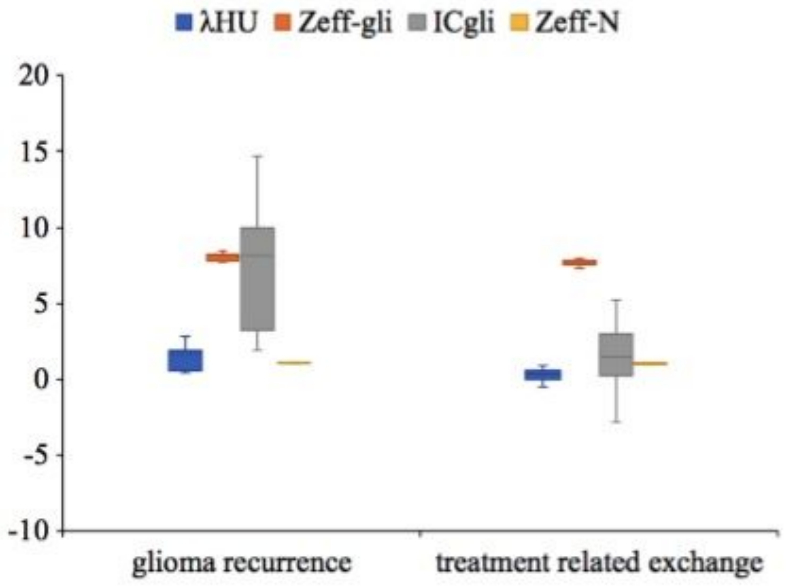

Figure 2

Box plots for glioma recurrence and treatment-related changes. The λHU, Zeff-gli, ICgli and Zeff-N measured in glioma recurrence were higher than in treatment-related changes in venous phase.

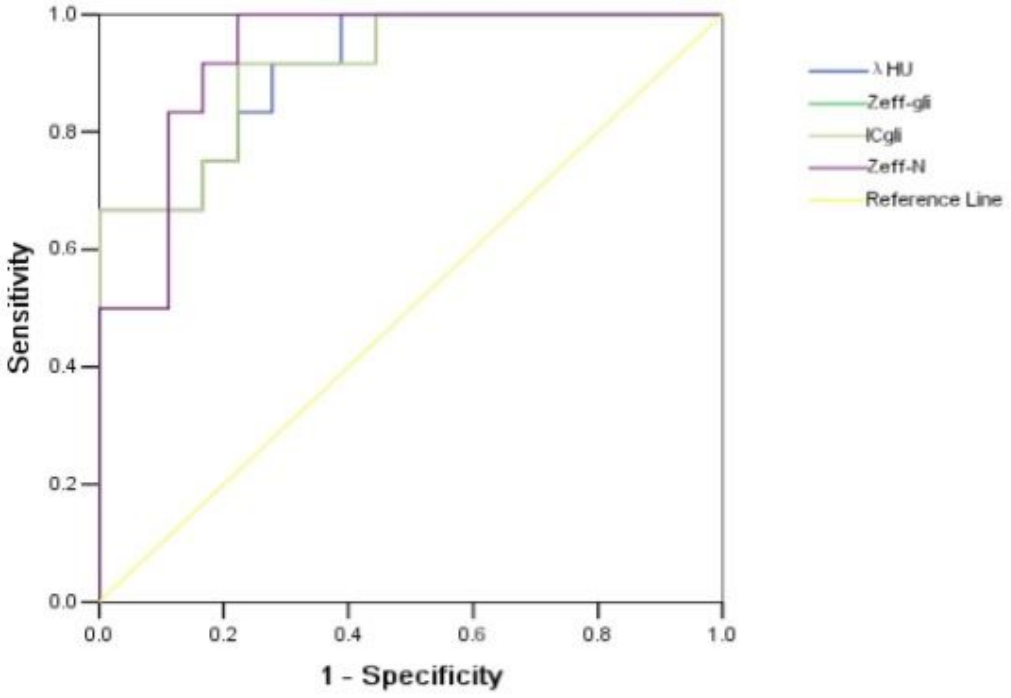

Figure 3

Graphs show receiver operating characteristic curves of λHU, Zeff-gli, ICgli and Zeff-N in venous phase for differentiating glioma recurrence from treatment-related changes in patients. The venous Zeff-N had the highest AUC (0.931), with the optimal threshold of 1.04. AUC = area under the curve